The Astrophysical Journal, 569:872–877, 2002 April 20

THE PHASE-RESOLVED X-RAY SPECTRA OF THE CRAB PULSAR

L. Zhang[1,2] and K. S. Cheng[1]

Received 2001 October 12; accepted 2001 December 26

ABSTRACT

We present a theoretical study of phase-dependent X-ray emission from the Crab pulsar. In the three-dimensional outer gap model for the Crab pulsar, X-ray emission is produced by synchrotron radiation of the secondary $e^{\pm}$ pairs, which is sensitive to the local properties of the emission regions, i.e., local magnetic field strength and local number $e^{\pm}$ density. We calculate X-ray pulse profiles for different energy bands and phase-dependent spectral indices of X-rays. We show that such a model can reproduce approximately the basic properties of the observed phase-dependent X-ray spectra of the Crab pulsar.

Subject headings: pulsars: individual (Crab Pulsar) — X-rays: stars

1. INTRODUCTION

The observations of X-ray emission from the Crab pulsar indicate that its spectral energy distribution is changing with its double-peak pulse profile. Pravdo, Angelini, & Harding (1997) analyzed the *RXTE* data between 5 and 250 keV and showed an evolution of the spectral index across the X-ray pulse in a reverse *s* shape. More accurate analysis was made by Massaro et al. (2000) with *BeppoSAX* observations. The basic observed properties are as follows: (1) a double pulse profile with a bridge separated by $\sim$0.4 in phase has been observed; (2) the spectra of two peaks soften and the softest spectrum is the first peak; (3) the spectrum of the interpeak region hardens with respect to the spectra of the two peaks; and (4) spectral indices are clearly increasing with energy over all the phase interval. The question is how to explain theoretically the phase-dependent properties of the observed X-ray emission from the Crab pulsar.

Based on the polar cap models of γ-ray emission (Daugherty & Harding 1996; Sturner & Dermer 1994), Pravdo et al. (1997) pointed out that the curvature radiation may be relatively more important than synchrotron radiation in the X-rays. However, there has not been a detailed calculation of the polar cap models yet. Massaro et al. (2000) have shown that a two-component emission model can account for the variation of pulse profile with energy and the phase change of the spectral index. They assumed that one component has the same profile observed in the optical, while the other presents a maximum at the phase 0.4 with the spectrum of the interpeak region and proposed that the latter can be originated in the outer magnetosphere, according to the outer gap models (Cheng, Ho, & Ruderman 1986a; Romani 1996). Although these authors proposed such a model, they did not give a complete model for the X-ray emission from the Crab pulsar.

Cheng, Ruderman, & Zhang (2000, hereafter CRZ) have considered a three-dimensional outer magnetosphere model of pulsars. In this model, the extensions of the outer gap along both radial and azimuthal directions are limited by photon-photon pair production. Assuming that the ratio of the total number of pairs at $r_{\rm lim}$ to that at the inner boundary of the outer gap ($r_{\rm in}$) equals 1/2, CRZ obtained the radial extension within which pair production takes place ($\sim 6r_{\rm in}$ for the Crab pulsar). In fact, this limit can be relaxed. In other words, we can relax the limits on the extensions along the radial and azimuthal directions by taking onto account the residual pairs produced inside the gap. In this paper, we will use this model to reproduce the pulse profiles for different energy bands and phase-dependent spectral indices of the X-ray emission from the Crab pulsar and show the limit of the observed data to this model. In § 2, we describe briefly the CRZ model and the modifications to this model. In § 3, we calculate the phase profiles and the spectral indices in different phase bins. Finally, we discuss our results in § 4.

2. THE PHOTON EMISSION MODEL

2.1. *The Structure of the Outer Gap*

According to the CRZ model, two outer gaps can exist in the open-field line volume of the pulsar magnetosphere. A three-dimensional outer gap is characterized by three quantities:

1. the fractional size, $f = h(r)/R_L$, of the outer gap at the distance to the pulsar, r, which is defined as the ratio of the vertical separation of the gap boundaries $h(r)$ in the (Ω, μ) plane to the light cylinder radius $R_L = c/\Omega$, where c is the light speed and Ω is the stellar angular velocity, P is the pulsar period, and μ is the magnetic moment;
2. the transverse (ϕ direction) extension of the gap $\Delta\phi = 2\pi\xi$;
3. the radial distance to the pulsar r.

We now briefly describe them as follows.

The outer gap is sustained by the $e^{\pm}$ pairs produced by X-ray and curvature photon collisions. Inside the gap, the electric field parallel to the magnetic field lines is approximated by CRZ as

$$E_{||}(r) = \frac{\Omega B(r) f^2(r) R_L^2}{cs(r)} , \qquad (1)$$

where $B(r)$ and $s(r)$ are the magnetic field and the curvature radius at the position r, respectively. Assuming, as usual, that the magnetic field in the outer magnetosphere is

[1] Department of Physics, University of Hong Kong, Pokfulam Road, Hong Kong, China.
[2] Department of Physics, Yunnan University, Kunming, Yunnan, China.

dipolar from the conservation of magnetic flux, i.e., $B(r)f^2(r) = \text{const}$, we have $f(r) \propto r^{3/2}$.

The electrons/positrons inside the outer gap are accelerated by the electric field given by equation (1). The energy of the $e^{\pm}$ pairs is limited by curvature radiation losses, and therefore their Lorentz factor is given by

$$\gamma_e(r) = f^{1/2}(R_L)\left[\frac{3}{2}\frac{\Omega B(R_L)R_L^3}{ec}\right]^{1/4}\left[\frac{s(r)}{R_L}\right]^{1/4}, \quad (2)$$

where $B(R_L)$ and $f(R_L)$ are the magnetic field and fractional size at the radius of the light cylinder R_L. These primary $e^{\pm}$ pairs lose their energy by radiating curvature photons with a typical energy

$$E_{\rm cur}(r) = f^{3/2}(R_L)\frac{3\hbar c}{2R_L}\left[\frac{3}{2}\frac{\Omega B(R_L)R_L^3}{ec}\right]^{3/4}\left[\frac{s(r)}{R_L}\right]^{-1/4}. \quad (3)$$

Therefore, if the typical energy of X-rays is E_{Xc}, the fractional size of the outer gap is estimated by photon-photon pair production condition $E_\gamma E_{Xc} \approx (mc^2)^2$. Zhang & Cheng (1997) have proposed a self-consistent outer gap model. In their model, the energy of the soft X-ray photons is determined by the backflow of the primary electrons/positrons from the outer gap, and the thermal X-rays with a typical temperature $T_s \approx 3.8 \times 10^6 f_0^{1/4}\xi^{1/4}B_{12}^{1/2}P^{-5/12}$ K emit from the stellar surface, where $f_0 = f(R_L/2)$. In this case, we see that f_0 is estimated as

$$f_0 = 5.5\ P^{26/21}\ B_{12}^{-4/7}\ \xi^{1/7}, \quad (4)$$

where $B_{12} = B_s/10^{12}$ G is the surface magnetic field strength in units of 10^{12} G and P is pulsar period in units of second. Here, ξ is still an unknown quantity. However, we see that f_0 is weakly dependent on ξ, which is likely of order of unity. In the first approximation, we assume $f_0 = 5.5\ P^{26/21}\ B_{12}^{-4/7}$. For the Crab pulsar, using equation (4), we have $f_0 \sim 0.04$. Because nonthermal X-rays will dominate for the Crab pulsar, Cheng, Ho, & Ruderman (1986b) have taken into account the effect of the soft photons emitted by the secondary pairs and showed that $f_0 \sim 0.05$ for the Crab pulsar. We will use $f_0 = 0.05$ below.

Quantity ξ determines the transverse extension of the outer gap. If there are no constraints, $\xi = 1$. In the CRZ model, ξ is limited by local photon-photon pair production processes. The number of curvature photons emitted at r per e^+/e^- per unit length in the outer gap is $N_\gamma = eE_{||}(r)/E_\gamma(r)$. For the Crab pulsar, the parallel electric field in the outer gap is $E_{||} \propto r^{-1/2}$ (Cheng, Ho, & Ruderman 1986b), which gives $E_\gamma(r) \propto r^{-1/8}$ after using the large r limit $s(r) = (rR_L)^{1/2}$ and $N_\gamma \propto r^{-3/8}$. Because E_γ is only weakly dependent on r, $\sigma_{\gamma\gamma}$ can be treated as constant over the pair production region. Therefore, the local optical depth is $\tau_{\gamma\gamma} = n_X(r)\sigma_{\gamma\gamma}l(r) \propto r^{-1}$, where $n_X = L_X\sigma/r^2E_X$ is the X-ray number density at r, L_X is the X-ray luminosity, and $l(r) \approx [2s(r)f(r)R_L]^{1/2}$ is the local optical path. Since the local pair production per unit length is $N_{e^\pm}(r) = (1 - e^{-\tau_{\gamma\gamma}})N_\gamma(r) \approx \tau_{\gamma\gamma}N_\gamma(r)$, CRZ have shown that pair production process mainly take places between $r_{\rm in}$ and $r_{\rm lim} \sim 6r_{\rm in}$ by requiring

$$\frac{r_{\rm lim}N_{e^\pm}}{r_{\rm in}N_{e^\pm}} \sim \left(\frac{r_{\rm lim}}{r_{\rm in}}\right)^{-3/8} = \frac{1}{2}. \quad (5)$$

Within the pair production regions, outgoing and incoming directions for particle flows are allowed. For $r > r_{\rm lim}$, only outgoing current is possible. For a given $r_{\rm in}$, ξ is determined by assuming the inner boundary radius $r_{\rm in}(\phi) = r_{\rm lim}$, which gives $\xi \approx 0.44$ or $\Delta\phi \approx 160^\circ$ (see Fig. 5 of CRZ). Of course, the condition (eq. [5]) is a little arbitrary because pair production processes exist for $[rN_{e^\pm}(r)]/(r_{\rm in}N_{e^\pm}) < 1/2$. This condition also limits the extension along the azimuthal direction, so the radiation in the azimuthal region (which eq. [5] has not satisfied) cannot be taken into account. CRZ mainly wanted to explain the phase-resolved γ-ray spectra from the main pulse (P1) to the interpulse (P2). Equation (5) is sufficient to cover the azimuthal extension between P1 and P2, which is about 40% of the entire period. More important, in the regions where $[rN_{e^\pm}(r)]/(r_{in}N_{e^\pm}) < 1/2$, $e^\pm$ pairs predominantly lose their energies via synchrotron radiation instead of inverse Compton scattering. Therefore, these regions contribute more to X-rays but less to γ-rays. We relax it in our computations below (§ 3).

Briefly, the structure of an outer gap is as follows. The fractional average height of the outer gap is given by f_0, the azimuthal extension is characterized by $\Delta\phi$ or ξ, and the radial extension of the radiation region is from $r_{\rm in}$ to R_L, but the photon-photon pair production is restricted to a relatively small region ($r_{\rm lim}$–$r_{\rm in}$).

2.2. *Radiation Region of Secondary Pairs*

In CRZ's model, thermal photon emission from the entire stellar surface is due to the bombardment of the backflowing charged particles from the outer gap and cyclotron resonance scattering. Nonthermal photons are produced by the synchrotron radiation of backflowing charged particles from the outer gap near the stellar surface and in a finite region just above the outer gap through a synchrotron self-Compton mechanism. If synchrotron photons produced by secondary pairs exceed the thermal photons from the surface, the pair production outside the gap is limited to a finite region, which depends on the mean free path of curvature photons in the synchrotron X-ray radiation field, i.e., $\lambda_{X\gamma}$. The number density of these low-energy photons is $n_X \sim L_{\rm gap}/\langle r\rangle^2 cE_X$, where $L_{\rm gap} \sim f_0^3 L_{\rm sd}$ is the total power radiated from the outer gap and $L_{\rm sd} \approx 3.85 \times 10^{31}\ P^{-4}\ B_{12}^2$ ergs s^{-1} is the spin-down power of the pulsar. Therefore, the mean free path for pairs production outside the outer gap is $\lambda_{X\gamma} \sim (n_X\sigma_p)^{-1}$, where $\sigma_p \sim \sigma_T/3$ is the pair production cross section and σ_T is the Thomson cross section. Using $\langle r\rangle \sim R_L/2$ and $E_X \approx (mc^2)^2/(f_0E_\gamma)$, we have

$$\lambda_{X\gamma} \sim 1.7 \times 10^{-3} f_0^{-4}\left(\frac{P}{0.1\ \rm s}\right)^5\left(\frac{E_\gamma}{10\ \rm GeV}\right)^{-1} B_{12}^{-2}\ R_L, \quad (6)$$

where $f_0 = 0.05$ and E_γ is given by equation (3). The corresponding pitch angle, $\beta(R_L/2)$ at $R_L/2$, is estimated as

$$\sin[\beta(R_L/2)] \approx \lambda_{X\gamma}/(R_L/2). \quad (7)$$

The radiation region of these secondary pairs can be estimated as follows. For a rotating oblique dipole field, polar cap shape defines the boundary of the open volume at the stellar surface for a given magnetic inclination. Because the outer gap is within the open volume, we divide all this volume into many parts, each of which intersects the stellar surface in an annular region with contours of the same shape of the polar cap, but with a smaller size (see Figs. 2 and 3 in CRZ). First, we determine the coordinate values (x_0, y_0, z_0)

of the last closed field lines at the stellar surface in units of the stellar radius. Then, the coordinate values (x_0', y_0', z_0') for different parts can be determined by using $x_0' = a_1 x_0$, $y_0' = a_1 y_0$ and $z_0' = \left[1 - (x_0'^2 + y_0'^2)\right]^{1/2}$ and by changing a_1. Since $a_1 = 1$ corresponds to the last closed field lines, we trace the magnetic field lines to find the values of a_1. The interval between the field lines and the last closed field lines at radius $R_L/2$ equals $\sim f_0$ (we label it as a_1^u), and the interval between the field lines and the field lines with a_1^u at radius $R_L/2$ equals $\sim \lambda_{X\gamma}/R_L$ (we label it as a_1^r). Therefore, the radiation region of the secondary pairs is the region whose upper and lower boundaries are characterized by a_1^u and a_1^r.

2.3. *Radiation Spectrum*

The secondary $e^{\pm}$ produce the nonthermal photons through a synchrotron self-Compton mechanism for the Crab pulsar. The distribution of the secondary pairs at the steady state can be expressed as

$$\frac{dN}{dE_e} = N_0(r)\left(\frac{E_e}{mc^2}\right)^{-2} \ln\left(\frac{E_{\rm cur}}{E_e}\right) \text{ for } E_{\rm min} \le E_e \le E_{\rm max} , \tag{8}$$

where $N_0(r)$ is the normalized factor and $E_{\rm min} \sim mc^2$ and $E_{\rm max} \approx E_\gamma/2$ are the minimum and maximum energy of the secondary pairs, respectively. Here we approximate $N_0(r)$ as follows. The local power into the curvature radiation from a single electron/positron is $l_{\rm cur} = eE_{||}c$, and the total number of charged particles in the outer gap under the thin gap approximation is $N \sim (\Omega\Phi/4\pi ce)R_L \sim \left[\Omega f(R_L)B(R_L)R_L^2\Delta\phi/4\pi ce\right]R_L$ (CRZ), where Φ is the magnetic flux. Therefore, the power into curvature radiation for N $e^{\pm}$ pairs is $L_{\rm cur} \sim N l_{\rm cur} \approx f^3(R_L)L_{\rm sd}(\Delta\phi/2\pi)[s(r)/R_L]^{-1}$. In this case, $N_0(r)$ is approximated as

$$\frac{N_0(r)}{(E_e/mc^2)^2} \approx \frac{1}{\dot{E}}\frac{L_{\rm cur}}{E_{\rm cur}} , \tag{9}$$

where $\dot{E} = (2/3)\left[e^4B^2(r)\sin^2\beta(r)/m^2c^3\right](E_e/mc^2)^2$ is electron energy loss into synchrotron radiation, and $\beta(r)$ is the local pitch angle which satisfies

$$\sin\beta(r) \sim \sin\beta(R_L)(r/R_L)^{\eta} . \tag{10}$$

Equation (10) comes from the following arguments. If we approximate the magnetic field lines by concentric circles with a local curvature radius $s(r)$, the pitch angle of secondary pairs satisfies $\tan\beta(r) \sim \sin\beta(r) \sim [2h'(r)/s(r)]^{1/2}$, where $h'(r)$ is the vertical distance from the emission field lines of the primary photons. If $h'(r)$ is proportional to the height of the gap, then $\sin\beta(r) \propto \{[R_L/s(r)]f(r)\}^{1/2}$. CRZ assumed the local curvature radius to be a dipolar form $s(r) \sim (rR_L)^{1/2}$, which gives $\sin\beta(r) \propto r^{1/2}$. However, $s(r)$ will not follow the dipolar form near the light cylinder, where the plasma kinetic energy density is comparable to the magnetic energy density. A more natural choice is $s(r) \sim R_L$, which gives $\sin\beta(r) \propto r^{3/4}$. We have calculated the X-ray spectra by using $\eta = 1/2$ and $\eta = 3/4$. Compared to the calculation results by using $\eta = 1/2$, the expected γ-ray spectra by using $\eta = 3/4$ are not changed because the γ-rays are mainly contributed by inverse Compton scattering, which does not depend on the pitch angle, but the expected X-ray spectra are changed slightly. Since most of the radiation will be emitted near the light cylinder, we present our results by using $\eta = 3/4$.

The photon spectrum of the synchrotron radiation of these secondary pairs is

$$F(E_\gamma, r) = \frac{\sqrt{3}e^3B(r)\sin\beta(r)}{mc^2h}\frac{1}{E_\gamma}\int_{E_{\rm min}}^{E_{\rm max}}\frac{dN(r)}{dE_e}F(x)dE_e , \tag{11}$$

where $x = E_\gamma/E_{\rm syn}$, $E_{\rm syn}$ is the typical energy of synchrotron radiation given by

$$E_{\rm syn}(r) = \frac{3}{2}\left(\frac{E_e}{mc^2}\right)^2\frac{\hbar eB(r)\sin\beta(r)}{mc} , \tag{12}$$

and $F(x) = x\int_x^{\infty} K_{5/3}(y)dy$, where $K_{5/3}(y)$ is the modified Bessel function of order 5/3. Because we only consider the X-ray emission from the Crab pulsar, we ignore the formulae of the spectrum of inverse Compton-scattered photons (see CRZ).

3. PHASE EVOLUTION OF X-RAY SPECTRA FROM THE CRAB PULSAR

For the Crab pulsar, $B_{12} = 3.8$ and $P = 0.033$ s, $f_0 = 0.05$, $\lambda_{X\gamma} \sim 0.12R_L$ by using equation (6), and $\sin[\beta(R_L)] \sim 0.4$ by using equations (7) and (10). In order to calculate the phase-resolved X-ray spectra from the magnetosphere of the Crab pulsar, we simulate the three-dimensional dipole magnetic field lines with retarded potential. For given inclination angle (α) and viewing angles (ζ), the emission morphology can be determined; CRZ used the inclination and viewing angles of 65° and 82°, respectively, to show the emission morphology and pulse profile of γ-rays. It does not mean that only these values can describe the emission morphology and pulse profiles. In our computations, we used these two values for reasons of consistency. We estimate the upper boundary of the secondary radiation region by using equation (6) for a fixed $f(R_L/2) = 0.05$, which is $a_1^r \sim 0.88$, then we trace the magnetic field lines in the three rotation magnetospheres and give the values of azimuthal angle ϕ, radial distance r, and the local magnetic field B in the range from the first open magnetic field lines ($a_1 = 1.0$) to the upper boundary of the secondary radiation region ($a_1^r = 0.88$) for the given viewing angle. Because of relativistic electrons/positrons in the outer gap, radiation occurs in the direction of motion of the electrons/positrons with a half-angle of $1/\gamma_e$. In such a geometry of three-dimensional magnetospheres, we can calculate the pulse profiles at different energy bands and the phase-dependent X-ray spectra. In our calculations, we have relaxed the condition in equation (5) to include the pairs, called residual pairs, produced beyond $(r_{\rm lim}N_{e^{\pm}}/r_{\rm in}N_{e^{\pm}}) = 1/2$ along the azimuthal direction. Most residual pairs have lower energies so that they contribute very little to high-energy γ-rays, which are mainly produced by inverse Compton scattering. However, they contribute more significantly to X-rays that are produced by the synchrotron radiation. Therefore, in this paper, we relax the condition in equation (5) to $(r_{\rm lim}N_{e^{\pm}}/r_{\rm in}N_{e^{\pm}}) \sim 2/5$. In our calculations, we divide the phase intervals into a number of bins, each one having a width of 5°.

3.1. *Pulse Profiles of X-Rays*

The observations at all wave bands show that the pulse profiles are dominated by two pulses, separated ~0.4 in pulse phase (e.g., see Kuiper et al. 2001). In X-ray bands, *ROSAT* and *BeppoSAX* observations provide more information to study the pulse profiles of X-rays from the Crab pulsar. From the *BeppoSAX* observations, a detailed study of the changes in the pulse profile shape has been made (Massaro, Feroci, & Matt 1997; Mineo et al. 1997). There are two main observed features: (1) the count rates of the second peak (P2) and bridge region (Ip) increase relative to that of the first peak (P1) for increasing energies, and (2) the shape width of the first peak increases with energy (also see Massaro et al. 2000; Kuiper et al. 2001). In order to quantify the variation of pulse shape with energy, the intensity ratios between the second peak and the first peak (P2/P1) and between the bridge region and the first peak (Ip/P1) in different energy ranges have been estimated (Massaro, Feroci, & Matt 1997; Mineo et al. 1997). It has been shown that P2/P1 and Ip/P1 increase with energy in X-ray range. Obviously, these observed features will give the limits to the model.

In order to calculate the pulse profiles in our model, we need to choose the inclination and viewing angles. As an example, we use the same values given by CRZ, i.e., $\alpha = 65^\circ$ and $\zeta = 82^\circ$. Further, we calculate the photon numbers per unit time (count rate) at the source by estimating integral X-ray spectra in each bin for a given energy range, i.e.,

$$\int_{E1}^{E2} F(E_\gamma, r) dE_\gamma \ , \tag{13}$$

where $F(E_\gamma, r)$ is given by equation (11), and E_2 and E_1 are the upper and lower limits for the given energy range. It should be noted that the observed count rates depend on the details of the detectors, so we normalized our expected pulse profiles to unity at the maximum of the first peak, which was done by Massaro et al. (2000). In Figure 1, we show the X-ray pulse profiles for three different energy bands (10–34, 15–80, and 80–300 keV), where the pulse profiles have been shifted along the phase and the first peak is set at zero phase. If we compare the expected count rates at the source with the observed data, our model can explain roughly the observed features of the pulse profiles for different energy bands, although there are some differences between them. From this figure, it has been shown that the pulse profile has a separation of ~0.4, that Ip and P2 increase with energy compared to P1, and that the width of P1 increases with energy.

We also calculate the X-ray spectra of P1, Ip, and P2, respectively. Following Mineo et al. (1997), the phase intervals are (−0.05, +0.05) for P1, (+0.05, +0.27) for Ip, and (+0.27, +0.47) for P2. We then estimate the flux ratios of P2 to P1 and Ip to P1. The results are shown in Figure 2. It is clear that the flux ratios of P2/P1 and Ip/P1 increase with energy, as shown by the observed data. However, compared to the observed data (Massaro et al. 1997; Mineo et al. 1997), the slopes of our results are more flat. In the *BeppoSAX* energy range, the maximum deviation of the model results from the observed data appears at low-energy range. For example, the expected P2/P1 at ~0.3 keV is ~1.19, which is greater than the observed value (0.95) by a factor of ~1.25, and the expected P2/P1 at ~144 keV is ~1.76, which is close to the observed value (~1.95).

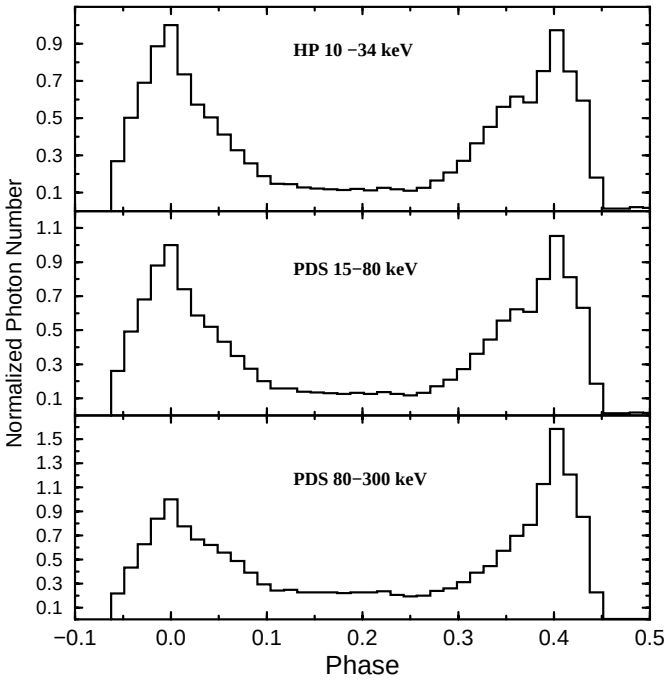

FIG. 1.—Expected X-ray pulse profiles of Crab pulsar for three different energy bands. The magnetic inclination and viewing angles are assumed to be 65° and 82°.

3.2. *Spectral Indices of X-Ray Spectra*

We now consider the phase-dependent spectral indices of X-ray spectra of the Crab pulsar. After calculating the phase dependent X-ray spectra, we use a single power law to fit the spectra for a given energy interval. Then we can obtain the expected phase-dependent spectral indices for different energy ranges. For a given energy band, the pulse profile and the spectral indices are calculated for the same bins, and the first peak is assumed to be at zero phase.

Massaro et al. (2000) analyzed *BeppoSAX* data to show the phase evolution of the spectral indices at different energy intervals (0.1–4.0, 1.6–10, 10–34, 15–80, and 80–300 keV).

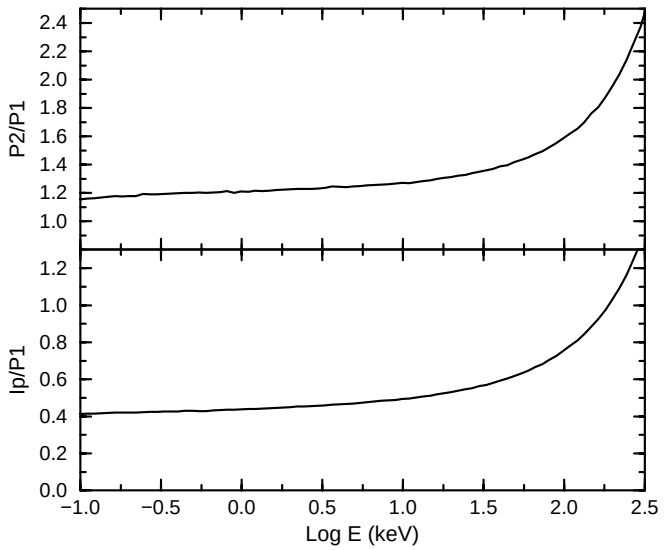

FIG. 2.—Expected flux ratios of peak two (P2) to peak one (P1) and interpeak region (Ip) to peak one (P1). The phase intervals are (−0.05, +0.05) for P1, (+0.05, +0.27) for Ip and (+0.27, +0.47) for P2.

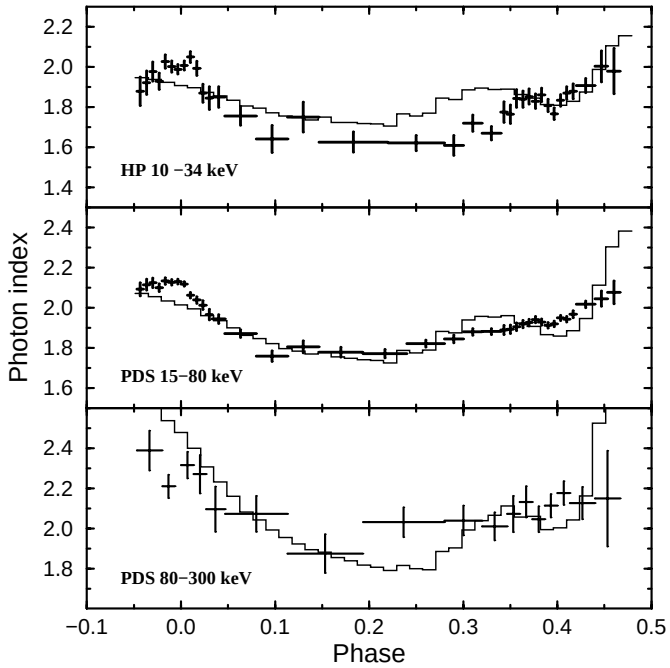

FIG. 3.—Comparison of expected spectral indices with the observed data. The magnetic inclination and viewing angles are assumed to be 65° and 82° for the Crab pulsar. The observed data are taken from Massaro et al. (2000).

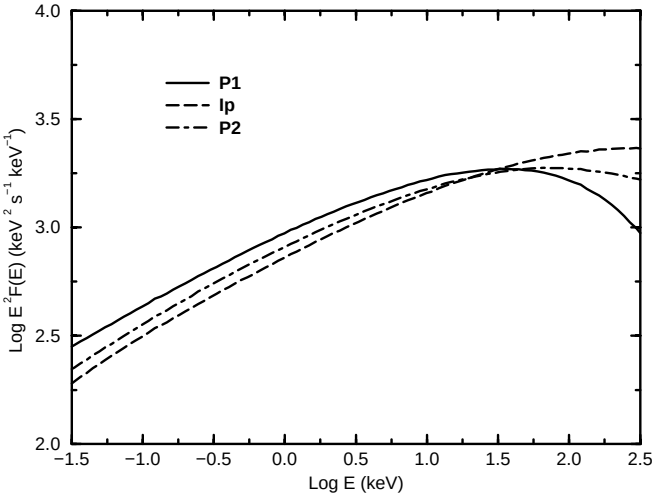

FIG. 4.—Expected average X-ray spectra of P1, Ip, and P2 for the Crab pulsar. The phase intervals of P1, Ip, and P2 are the same as those in Fig. 2.

Because of the interstellar absorption at low-energy range below a few keV, the spectral index depends on the hydrogen column density in the Crab direction. However, this column density is uncertain and literature estimates vary from 3.3×10^{21} to 3.6×10^{21} cm^{-2} (Kuiper et al. 2001). In order to avoid the interstellar absorption effect, we do not compare our expected results with those observed at energy intervals of 0.1–4.0 and 1.6–10 keV. In Figure 3, we show the comparison of our model results with observed data at the energy intervals of 10–34, 15–80, and 80–300 keV. From Figure 3, our model results give a phase dependence of the spectral indices similar to observed data, i.e., P1 has the softest spectrum, while the middle of bridge region is the hardest, and spectral indices are clearly increasing with energy in all the phase intervals. In Figure 3, there are some differences between the observed data and the model results. The expected spectral indices vary monotonically across the first peak, which is not consistent with the observed data. One possible explanation is that the emission process responsible for the first peak is not only the synchrotron radiation from the secondary pairs. In the low-energy range (e.g., 10–34 keV), the expected indices in the bridge range are greater than the observed indices. According to our model, the X-rays are produced in both regions; one is close to the inner boundary, which emits X-rays with a flat spectrum, and another is close to the light cylinder, which emits X-rays with a steep spectrum. In Figure 4, we show the average spectra of P1, Ip, and P2 expected in our model. It is very clear that the spectrum of P1 is the softest and that the spectrum of Ip is the hardest.

4. DISCUSSION

We have shown that the observed features of phase-dependent X-ray spectra of the Crab pulsar can be explained roughly by the CRZ model. After the magnetic inclination and viewing angles are determined for the Crab pulsar, the basic parameters are the magnetic field and the pulsar period in this model. According to this model, the X-rays at the first peak are produced by the synchrotron radiation at a range of $r/R_L \sim 0.6$–1.4. As the phase increases, the X-rays at the bridge region are mainly produced by synchrotron radiation in the region of $r/R_L \sim 0.2$–0.6, plus a small contribution from the radiation in the larger distance region ($r/R_L \geq 1$). Near the second peak (the region from $\sim$0.3–0.35), the contributions from the region close to the inner boundary and from the large distance region $r/R_L \geq 0.6$ are comparable, which results in the increase of the spectral indices. For the X-rays in the second peak, the radiation is mainly from the region of $r/R_L \sim 0.2$–0.6. Therefore, there is a weak peak for the spectral indices at the phase of $\sim$0.35.

In this model, we have calculated the pulse profiles and phase-dependent spectral indices for different energy bands (see Figs. 1 and 3). We have also estimated the flux ratios of P2/P1 and Ip/P1 (Fig. 2) and the X-ray spectra of P1, Ip, and P2, which resulted in approximate agreement with the observed data. However, there are also some differences between the model results and the observed data. For the pulse profiles, although our model can reproduce roughly the observed features, the extents of Ip and P2 relative to that of P1 are slightly different from the observed. In the low-energy range, expected Ip/P1 is larger than the observed one (see Fig. 2). Furthermore, there are some differences between the expected spectral indices and the observed data. Besides the fact that the expected spectral indices in the phase range of 0.3–0.35 are larger compared to the observed data, the expected spectral indices in the lower energy range (10–34 keV) cannot fit the observed well. These differences indicate that our model needs a more detailed treatment. In fact, in our simplified model, the X-ray emission of the Crab pulsar is assumed to be mainly the synchrotron radiation from the secondary pair radiation region, and the photons are assumed to be emitted tangent to the local magnetic field lines, but particles with large initial pitch angles may emit in other directions. The X-ray emission in our model is sensitive to the local properties of the emission regions, such as the magnetic field strength, the

$e^{\pm}$ number, $e^{\pm}$ density, and the pitch angle of radiating pairs.

In our calculations, we have used the values of magnetic inclination (α) and viewing angles (ζ) given by CRZ. In fact, there may be other value of these two parameters which can account for the observed properties of emission from the Crab pulsar. Up to now, these two parameters have not been determined from the observations. From radio observations, Rankin (1993) estimated that $\alpha \approx 84^\circ$ and ζ is not known. Moffett & Hankins (1999) used the polarimetric observations of the Crab pulsar at frequencies between 1.4 and 8.4 GHz to estimate $\alpha \approx 56^\circ$ and $\zeta \approx 117^\circ$. Optical observations show $\alpha = 86^\circ$ and $\zeta \approx 74^\circ$ (Narayan & Vivekanand 1982). Romani & Yadigaroglu (1995) estimated the values of α and ζ in their outer gap model as $\alpha = 80^\circ$ and $\zeta = 62^\circ$.

It should be pointed out that the main purpose in this paper is to explain the phase-dependent X-ray spectra of the Crab pulsar. According to the CRZ model, the nonthermal radiation from the Crab pulsar is produced from the synchrotron self-Compton mechanism. High-energy γ-ray emission is mainly produced by the Compton scattering. Cheng et al. (2000) have used this model to explain the phase-dependent spectra and phase-average spectrum of high-energy γ-rays for the Crab pulsar. Therefore, in principle, our model can explain nonthermal radiation from X-rays to γ-rays. Since our three-dimensional model is based on a rotating vacuum dipole, while the realistic pulsar magnetosphere is filled with relativistic plasma, some discrepancies are expected between model results and the observed data. However, we believe that this three-dimensional model can explain most observed phase-dependent features from X-rays to γ-rays of the pulsar. In addition to the Crab pulsar, we have applied this three-dimensional model to other pulsars and obtained reasonable agreements (Zhang & Cheng 2000, 2001). Recently, Kuiper et al. (2001) presented the observed phase-dependent features from soft X-rays up to high-energy γ-rays of the Crab pulsar. The detailed study of multiwave band, phase-dependent spectra from the Crab pulsar are needed.

We thank T. Mineo for providing us with *BeppoSAX* X-ray data from the Crab pulsar and the referee, E. Massaro, for his constructive comments. This work is partially supported by an RGC grant of the Hong Kong Government, the National Nature Scientific Foundation of China (10073008), and the National 973 Projection of China (NKBRSFG 19990754).

REFERENCES

Cheng, K. S., Ho, C. & Ruderman, M.A. 1986a, ApJ, 300, 500
———. 1986b, ApJ, 300, 522
Cheng, K. S., Ruderman, M., & Zhang, L. 2000, ApJ, 537, 964
Daugherty, J. K., & Harding, A. K. 1996, ApJ, 458, 278
Kuiper, L., et al. 2001, A&A, 378, 918
Massaro, E., Cusumano, G., Litterio, M., & Mineo, T. 2000, A&A, 361, 695
Massaro, E., Feroci, M., & Matt, G. 1997, A&AS, 124, 123
Mineo, T., et al. 1997, A&A, 327, L21
Moffett, D. A., & Hankins, T. H. 1999, ApJ, 522, 1046
Narayan, R., & Vivekanand, M. 1982, A&A, 113, L3
Pravdo, S. H., Angelini, L., & Harding, A. K. 1997, ApJ, 491, 808
Rankin, J. M. 1993, ApJS, 85, 145
Romani, R. W. 1996, ApJ, 470, 469
Romani, R. W., & Yadigaroglu, I.-A. 1995, ApJ, 438, 314
Sturner, S. J., & Dermer, C. D. 1994, ApJ, 420, L79
Zhang, L., & Cheng, K. S. 1997, ApJ, 487, 370
———. 2000, A&A, 363, 575
———. 2001, MNRAS, 320, 477